Hindawi
International Journal of Antennas and Propagation
Volume 2017, Article ID 9750257, 9 pages
https://doi.org/10.1155/2017/9750257

Research Article

Miniaturized Circularly Polarized Implantable Antenna for ISM-Band Biomedical Devices

Ke Zhang, Changrong Liu, Xueguan Liu, Huiping Guo, and Xinmi Yang

School of Electronic and Information Engineering, Soochow University, Suzhou, Jiangsu 215000, China

Correspondence should be addressed to Changrong Liu; crliu@suda.edu.cn

Received 31 October 2016; Revised 16 February 2017; Accepted 12 March 2017; Published 30 March 2017

Academic Editor: Symeon Nikolaou

A compact circularly polarized antenna operating at 915 MHz industrial, scientific, and medical (ISM) band for biomedical implantable applications is presented and experimentally measured. The proposed antenna can be miniaturized to a large extent with the compact size of $15 \times 15 \times 1.27$ mm^3 by means of loading patches to a ring-shaped microstrip patch antenna. An impedance bandwidth of 10.6% (865–962 MHz) for reflection coefficient less than −10 dB can be obtained. Meanwhile, the simulated 3 dB axial-ratio (AR) bandwidth reaches 14 MHz. Finally, the optimized design was fabricated and tested, and the measured results agree well with simulated results.

1. Introduction

With the rapid development of wireless communication applications in contemporary biomedical domains, implantable devices play a critical role in communicating robustly with external devices. Therefore, implantable antennas have been rising public horizons for their peculiarities of obtaining and storing real-time data [1, 2]. However, because of its special implanted condition, the fundamental requirement of compact size must be well met. Beyond that, the characteristic of circular polarization can be realized due to its advantages of reducing multipath loss and problems-solving of polarization mismatching. In this case, receiving antennas can effectively react to transmitting antennas with varying orientations.

Many groups have been concentrating on doing researches on implantable antennas. In order to satisfy the basic requirements of miniaturization, there are many technologies to be adopted to attain a good result of downsizing. Cutting slots in the radiator patch or the ground plane [3] can efficaciously extend current path, which can have a reduction in size distinctly. In [4], an H-shaped cavity slot antenna implanted in human body was designed. Loading shorting strips or pins [5] can implement standing wave structure from open to short circuit, which can shrink the size by half. The multilayer structure of antenna was adopted for the measurement of implantable wireless communication systems [6, 7]. Planar inverted-F antennas (PIFA) have arrived at a deep level by the endeavor of many groups [8, 9]. Loading capacitive/inductive stubs can also enhance the capacitive/inductive couplings to reduce the size with fixed operating frequency [10]. Simultaneously, since circular polarization can reduce the multipath loss and improve bit-error-rates compared to liner polarization, it has a practical significance for implantable antennas. Meanwhile, circular polarization (CP) can be realized by truncating a pair of corners to produce perturbation. Also, employing the forms of two or more feeds to generate orthogonal modes for CP operation can also readily achieve circular polarization. Generally speaking, the crux of generating circular polarization is to produce appropriate perturbation.

In this work, a compact circularly polarized patch antenna operating at 915 MHz is proposed. The work focuses on the analysis of design procedure and measurement of the proposed antenna. A homogenous cube phantom with skin equivalent dielectric properties is established for mimicking human subcutaneous environment. By the way of truncating corners to protrude disturbance elements, along with the optimization of feed location on the y-axis, the circular polarization operation can be realized expediently. The details of the proposed antenna design and correlative measurements are described and discussed.

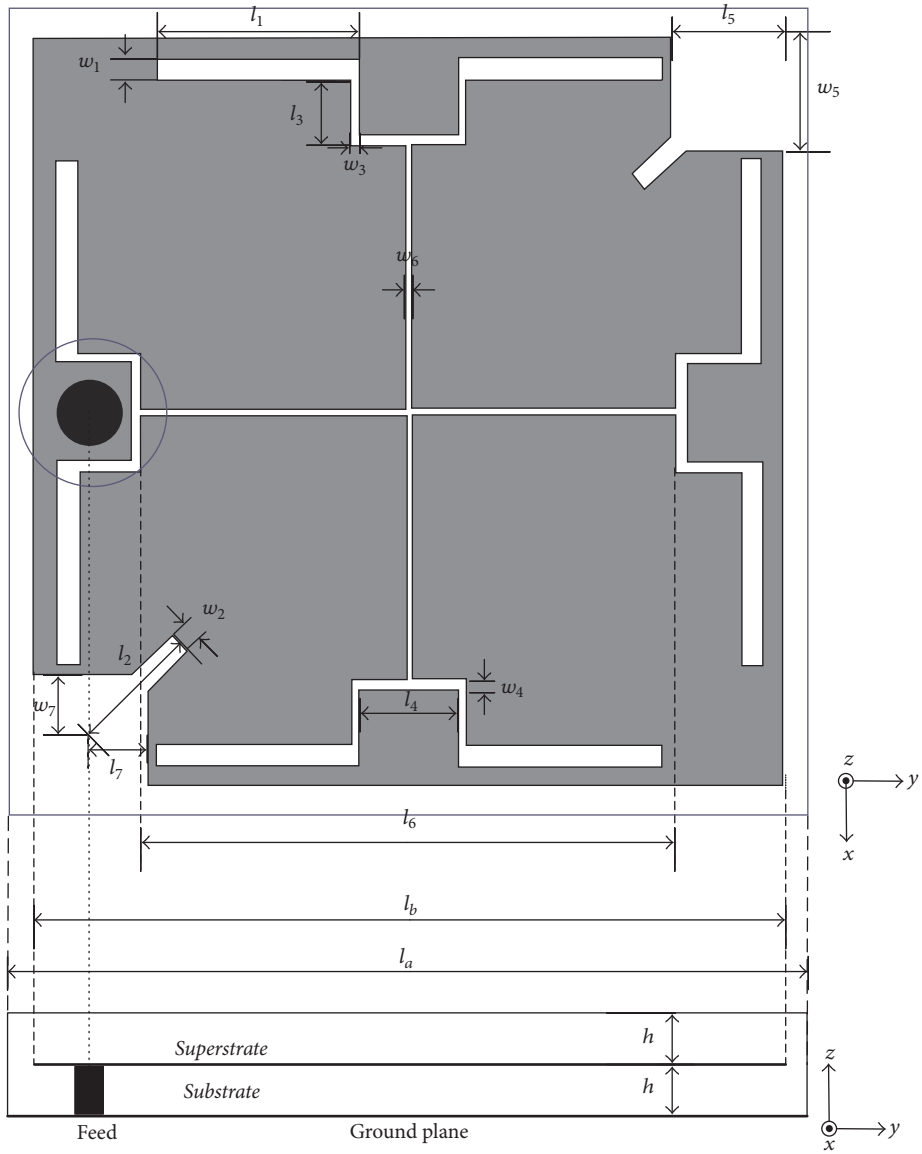

Figure 1: Geometry of the proposed circularly polarized antenna.

2. Structure of the Proposed Antenna

As shown in Figure 1, the configuration of the proposed CP antenna for implantable applications is depicted. The structure of the proposed CP antenna is square and includes patch and ground plane printed on the substrate of the Rogers 3010 with a dielectric constant of 10.2 and a loss tangent of 0.0035. The distance from the original point to the feed location is 5.97 mm and the feed is positioned on the y-axis. Meanwhile, the square size of both the proposed antenna and the ground plane is fixed to 15 × 15 mm. The distance from the edge of the radiator patch to the side of the substrate is 0.5 mm. The 0.635 mm thick superstrate with the identical size of substrate is made from the same material (Rogers 3010). A cube with the dimension of $100 \times 100 \times 60$ mm^3 is established to be ana logous to human skin subcutaneous environment. Figure 2 describes the permittivity and conductivity as a function of frequency and the dielectric properties of the skin phantom model at 915 MHz are $\varepsilon_r = 41.35$ and $\sigma = 0.87$ S/m [13]. It is worth noting that the implantable radiator lacks high efficiency, which is caused mainly by the compact radiating area and loss of human environment. Note that the implanted depth is 4 mm, which is the distance from the patch to the edge of skin phantom. The detailed parameters are listed in Table 1.

3. Analysis of Miniaturization and Circular Polarization

3.1. Configuration of the Circularly Polarized Implantable Antenna. Broadly speaking, the proposed antenna adopts the structure of loop antenna, which is composed of a radiator patch, cross slots, a pair of square truncated corners, extra diagonal perturbation elements, and a ground plane.

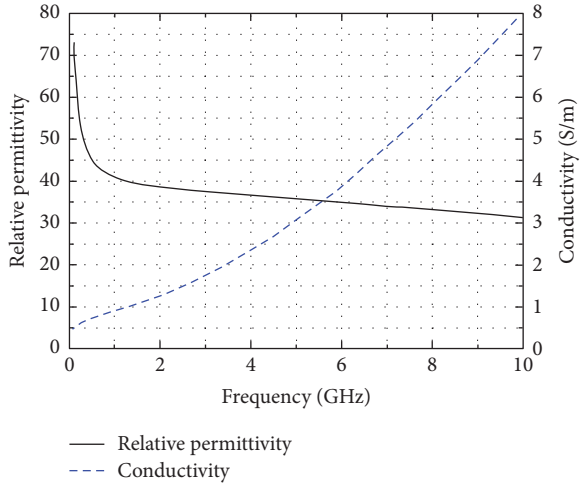

Figure 2: The dielectric properties of the skin tissue in simulation.

Table 1: Detailed parameters of the proposed antenna.

Symbol	Value (mm)
l_1	3.8
l_2	2.42
l_3	1.2
l_4	1.85
l_5	2.1
l_6	5
l_7	1.1
l_a	15
l_b	14
w_1	0.4
w_2	0.4
w_3	0.16
w_4	0.2
w_5	2.1
w_6	0.1
w_7	1.1

The reason why we utilize the loop structure is that the current can be pushed to flow along the edge, which can greatly lengthen the effective current path. Figure 3 gives three vivid types to explain the miniaturized mechanism concerning extending current path. The current path of the structure of case 1, a simple patch antenna equivalent to be half-wavelength transmission line, is longer than the structure of case 2 consisting of a square ring. The use of a square ring leads to the result of extending the effective current flowing path [14], which is similar to the increase of wavelength. To further obtain a compact size, we adopt the method of loading stubs.

Since antenna can be regarded as a transmission line, we can regard case 3 as four transmission lines with loading stubs, as shown in Figure 4(a). Figure 4(b) describes the corresponding equivalent circuit, where L_1 and C_1 are the inductance and capacitance of a transmission line. C_2, L_2, C_3, and L_3 stand for the inductance and capacitance of high impedance line and patch, respectively. It is well known that introducing the LC loading would become slow wave structure and contribute to the miniaturization. Thereby, it is obvious to witness the reduction of the size.

From another aspect, for a brief illustration, the proposed antenna can be miniaturized by loading stubs, which can be analyzed by introducing ABCD matrix [15]. Compared with the transmission line shown in Figure 5(a) (path: c-d), the proposed antenna can be considered to be composed of transmission lines consisting of loading stubs. The electrical length of $\lambda/4$ transmission line equals to $\pi/2$; nevertheless, we can get the electrical length (path: g-h) of the proposed antenna less than $\pi/2$ by calculation.

Meanwhile, to provide a persuasive illustration, we compare the sizes of the proposed antenna and the single loop antenna operating at the same frequency of 915 MHz. We spilt each of the above structures into two parts and simulate them in the way of putting two lumped ports to get the phase difference. The phase difference of Figure 5(a) is 174 degrees (path: a-b), and the difference of Figure 5(b) is 178 degrees (path: e-f). The physical length of the proposed antenna is 15 mm, while the physical length of the conventional antenna is 31 mm. That is to say, the proportion of area reduction reaches approximately 1/4, which can account for miniaturization vividly.

It is noteworthy that the initial construction of the implantable antenna has linear polarization, and the performance of CP can be achieved by truncating corners in this structure. In order to guarantee the 3 dB axial-ratio bandwidth, more widespread disturbance should be produced. Therefore, pairs of diagonal rectangle slots ($l_5 \times w_5$) and extra slots ($l_2 \times w_2$) are used to react to circular polarization. It turns out that the modification of feed location would also have an effect on the axial-ratio performance. After optimization, the position of feeding point is fixed at 0 mm, −5.97 mm, and 0.635 mm in the three-dimensional coordinate system.

3.2. Biocompatible Insulation. In realistic applications, the proposed antenna must be biocompatible with the surrounding tissue. There are two typical approaches to deal with the biocompatibility insulation issue in practical applications. One is to make biocompatible materials such as Macor, Teflon, and Ceramic Alumina [16] directly attach on the antennas. We replace the Rogers RO3010 by biocompatible alumina (Al_2O_3) ceramic ($\varepsilon_r = 9.8$). That is to say, if biocompatible, the substrate and superstrate should be both replaced. From Figure 6, we can see that the resonant frequency will shift from 915 MHz to 930 MHz and the axial ratio will get worse, which is caused by the different dielectric constant. In future work, we can optimize the proposed antenna with biocompatible substrate and superstrate.

The other way is encasing the antenna with a thin-layer coating with low-loss biocompatible material [17]. It is noted that the thickness of coating should be codesigned.

3.3. The Specific Absorption Rate (SAR) Evaluation. For the implantable antenna, the issue of radiation when patients are exposed to electromagnetic field should be given sufficient

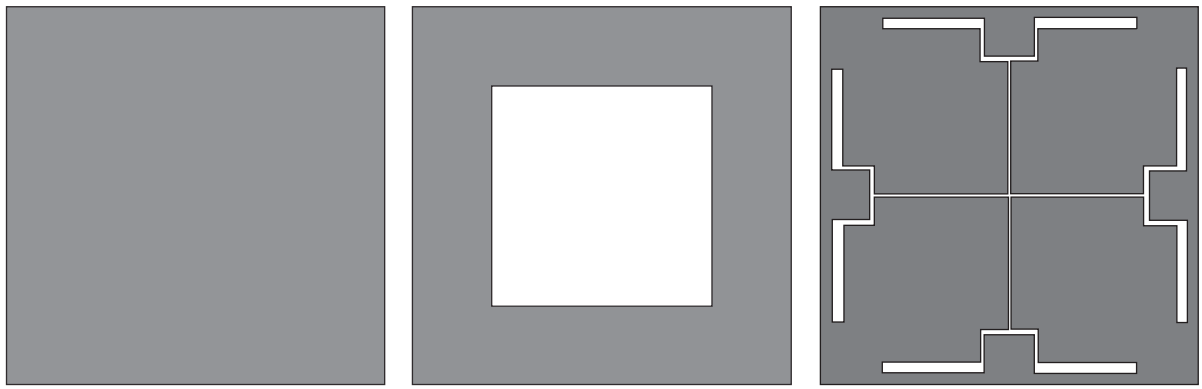

Figure 3: Three types of implantable microstrip patch antenna cases.

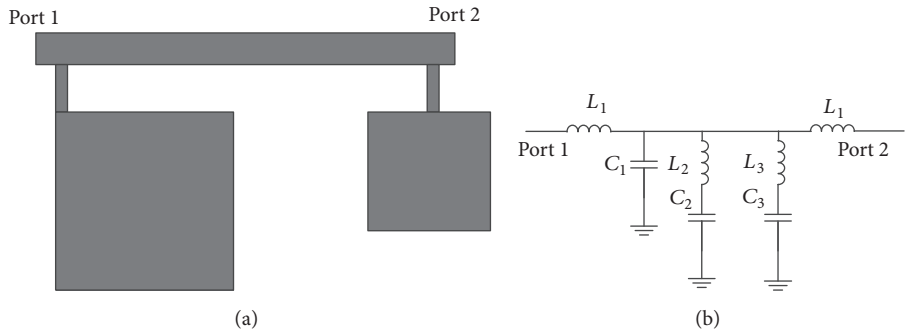

Figure 4: Transmission line with loading: (a) structure; (b) equivalent circuit.

concerns. Maximum SAR value is confined to defend radiation. The IEEE C95.1-1999 standard sets strict restrictions on the SAR, which regulates that the SAR averaged over any 1 g of tissue should be limited to 1.6 W/Kg.

When the transmitter power of the proposed antenna is set to be 1 W, the simulated maximum 1 g average SAR value is 517 W/kg. Thus, the transmitter power delivered to the proposed implantable antenna cannot exceed the regulation of 3.1 mW (~4.9 dBm) to meet the IEEE standard of 1 g average SAR maximum value. In this work, the output power for the transmit chip is −19 dBm, which is much lower than the maximum permitted power. In this condition, the issue of safety should not be a concern.

4. Simulated and Measured Results

In order to make an intuitive understanding, we contrast the proposed antenna and the conventional patch antenna with perturbations, as shown in Figure 7. The conventional antenna undergoes the structure of patch antenna in the same dimension, adding a pair of corners in the center square slot. The proposed antenna operates at 915 MHz; nevertheless, the conventional loop patch antenna works at 2.6 GHz. The shift of the frequency can be akin to the change of size and we can conclude that the reduction of size can reach 65% if replacing the conventional patch antenna at a fixed operating frequency. From Figure 8, we can see that the proposed antenna has a good circular polarization property at ISM band. The valley ratio of AR can reach 1.3 dB, which basically meets the requirement.

Figure 9 shows the simulated radiation patterns of the proposed antenna operating at 915 MHz in human skin phantom. The maximum realized gain reaches −27 dBic, which is simulated under the circumstances of the implanted depth of approximate 4 mm. It should be noted that the gain would be influenced by the variation of depth and the size of cubic skin phantom. Also, from the figure, we can understand that the kind of main polarization of the antenna is right-handed circular polarization (RHCP). The cross-polarization discrimination of the antenna radiating at primary radiation direction reaches 20 dB.

To illustrate vividly the radiation mechanism, Figure 10 describes the current directions varying with the time by changing the steps of $T/4$. Strong currents appear at the left and right edge of patch and flow along $+x$-axis at $t = 0$. The currents mainly concentrating on the upper and down parts of patch flow towards $+y$-axis when at $t = T/4$. Then, the directions of strong currents at $t = T/2$ and $t = 3T/4$ are opposite to those at $t = 0$ and $t = T/4$. We can see from the figure that the currents orientations rotate in anticlockwise directions to yield right-hand circular polarization (RHCP).

In order to confirm the validity of simulation results, the proposed antenna was fabricated and measured in a beaker filled with homogeneous mixture solution mimicking

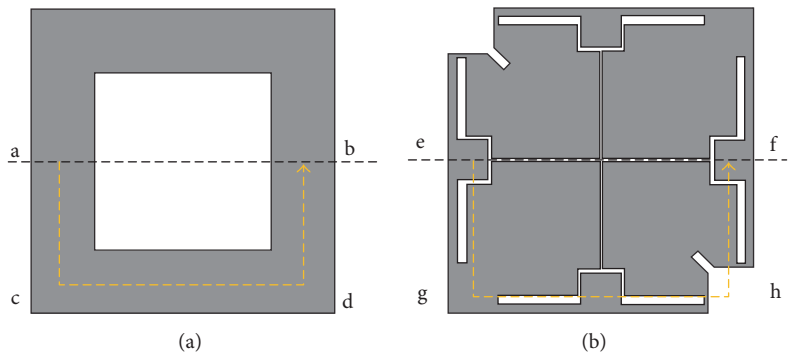

Figure 5: The comparison of loop antenna and the proposed antenna (not in scale).

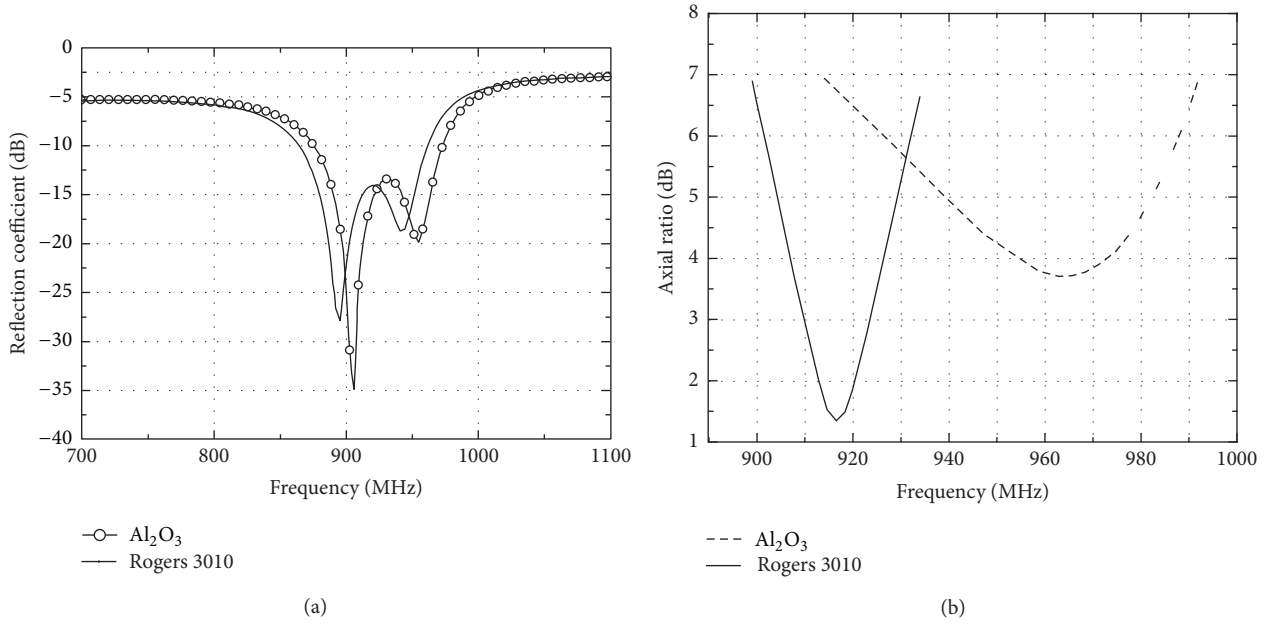

Figure 6: The comparison of the proposed antenna with different materials: (a) reflection coefficients; (b) axial ratio.

approximately subcutaneous environment. The recipe of the liquid is found to be 42% deionized water, 1.5% salt, and 56.5% sugar by weight [18]. Figure 11(a) shows the photograph of fabricated antenna and Figure 11(b) shows the measurement setup of communication link between the implantable antenna and the external dipole. We measure the CP property by comparing the transmission coefficient between transmit antenna (Tx) and receive antenna (Rx) with various orientations. In this measurement, the reception of dipole antenna can reflect the polarization of the proposed antenna.

As seen in Figure 12, S-parameters of the proposed antenna and the dipole are simulated and measured, respectively. Because of the possible fabricated tolerance, the measured reflection coefficient of the designed antenna less than −10 dB ranges from 874.2 MHz to 926.35 MHz (5.7%). The dipole operates at 915 MHz with the 22.8% relative bandwidth. The discrepancy of the shift of frequency may be mainly caused due to the unavoidable gap between substrate and superstrate. The transmission coefficient of the two antennas was also simulated and measured as the positioned angles of dipole were altered. We can see that the good polarization is well achieved at around 915 MHz ($|S_{21}|[\text{phi} = 0^\circ] \cong |S_{21}|[\text{phi} = 90^\circ]$). There is no apparent difference in the $|S_{21}|$ value when the dipole antenna is placed at different degrees. Certainly, the distance of two antennas should not be far. And the CP property of the proposed antenna can be calculated by the comparison of the communication link levels for two orthogonal polarization processes.

5. Communication Link

Considering the uplink communication, we assume an antenna, placed apart further, operating at 915 MHz in free space as the receiver antenna to assess the communication distance. And the implantable antenna embedded in the related environment can be considered to be the transmit antenna. The distance between transmitter and receiver can

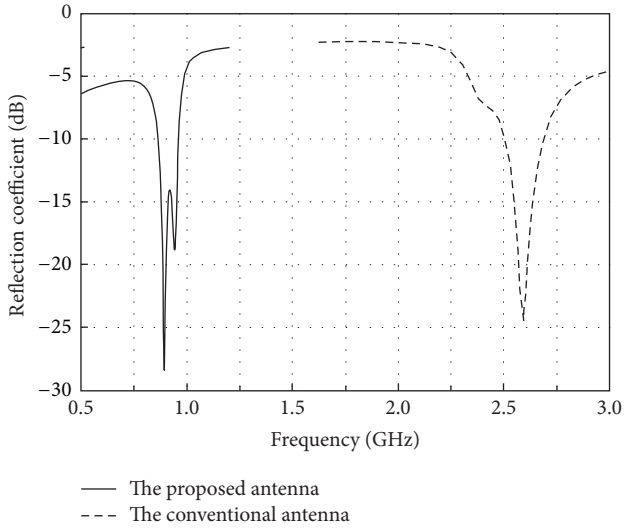

Figure 7: The comparison of the proposed antenna and the conventional antenna.

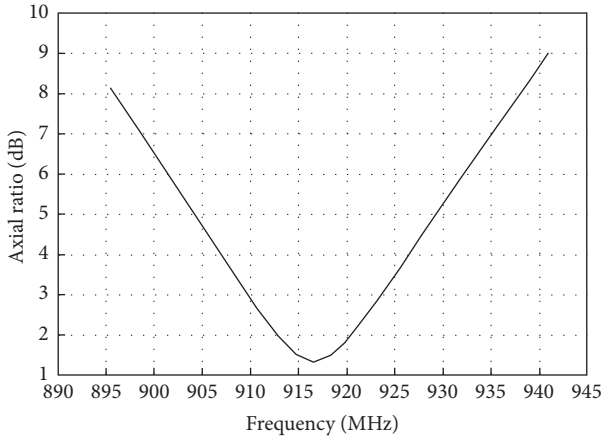

Figure 8: Simulated axial ratio of the proposed antenna.

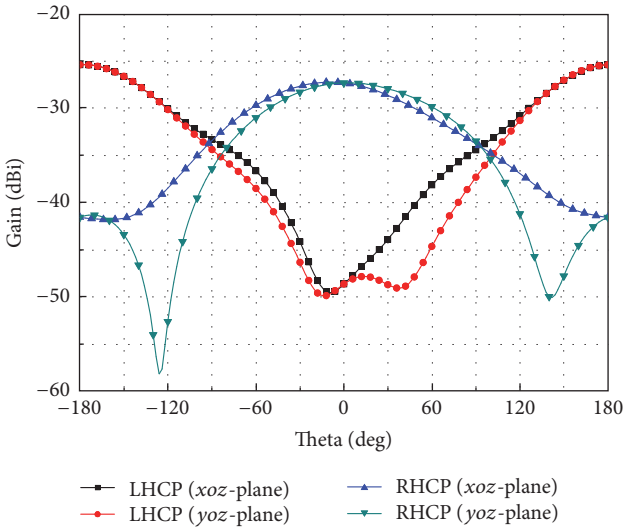

Figure 9: Radiation patterns of the proposed antenna.

Table 2: Parameters of the link budget.

Frequency	915 MHz
Tx power Pt	−19 dBm
Tx antenna gain Gt	−27 dBi
Tx antenna gain Gr	2.15 dBi
Rx antenna polarization	CP
Receiver noise floor RNF	−101 dBm
SNR (BER = $1E-5$)	14 dB

be denoted by d. The communication link margin (LM) can be described in terms of the following:

$$\mathrm{LM} = P_t - L_f + G_r + G_t - \mathrm{SNR} - \mathrm{RNF} \tag{1}$$

$$L_f = 20 \lg\left(\frac{4\pi d}{\lambda}\right), \tag{2}$$

where P_t is the input power of the transmit antenna, L_f donates the path loss in free space, G_t is the transmit antenna gain, and G_r is the gain of the receive antenna. RNF is the receiver noise floor, and the SNR is the signal to noise ratio.

The impedance mismatch can be described as follows:

$$L_{\mathrm{imp}}\ (\mathrm{dB}) = -10 \log\left(1 - |\Gamma|^2\right), \tag{3}$$

where Γ represents the reflection coefficient.

It is worthwhile noting that $|S_{11}|$ of the proposed antenna at 915 MHz reaches −14.5 dB; thus, the impedance mismatch loss equals 0.157 dB at 915 MHz. The little mismatching loss plays the insignificant role, which can be neglected. Meanwhile, we can consider the exterior antenna with the realized gain of 2.15 dBi as the receiver antenna. The polarization of the exterior antenna can result in different impedance mismatch losses. Assuming that the exterior receive antenna is with circular polarization, the mismatch loss of which is 0 dB. Yet the matching loss of liner polarized antenna is 3 dB. The values of SNR and RNF are obtained from [19], and the link margin can be calculated by the parameters listed in Table 2.

Figure 13 shows the detailed relationship of link margin with varying distance according to (1). To realize wireless communication robustly, we must guarantee that the link margin must be higher than 0 dB. From the simulated link margin of the proposed CP implantable antenna, we can conclude that only when the distance between Tx and Rx antenna with CP is less than around 3.8 m can we make the wireless communication possible. What is more, when the receiver antenna is with liner polarization, the communication distance will become shorter.

6. Conclusion

A miniaturized circularly polarized antenna for biomedical applications operating at 915 MHz has been presented in this work. By the way of analyzing the miniaturized technologies of several antennas, as described in Table 3, we can compare each performance to obtain advantages of the above examples. The compact antenna with the advantage of no shorting

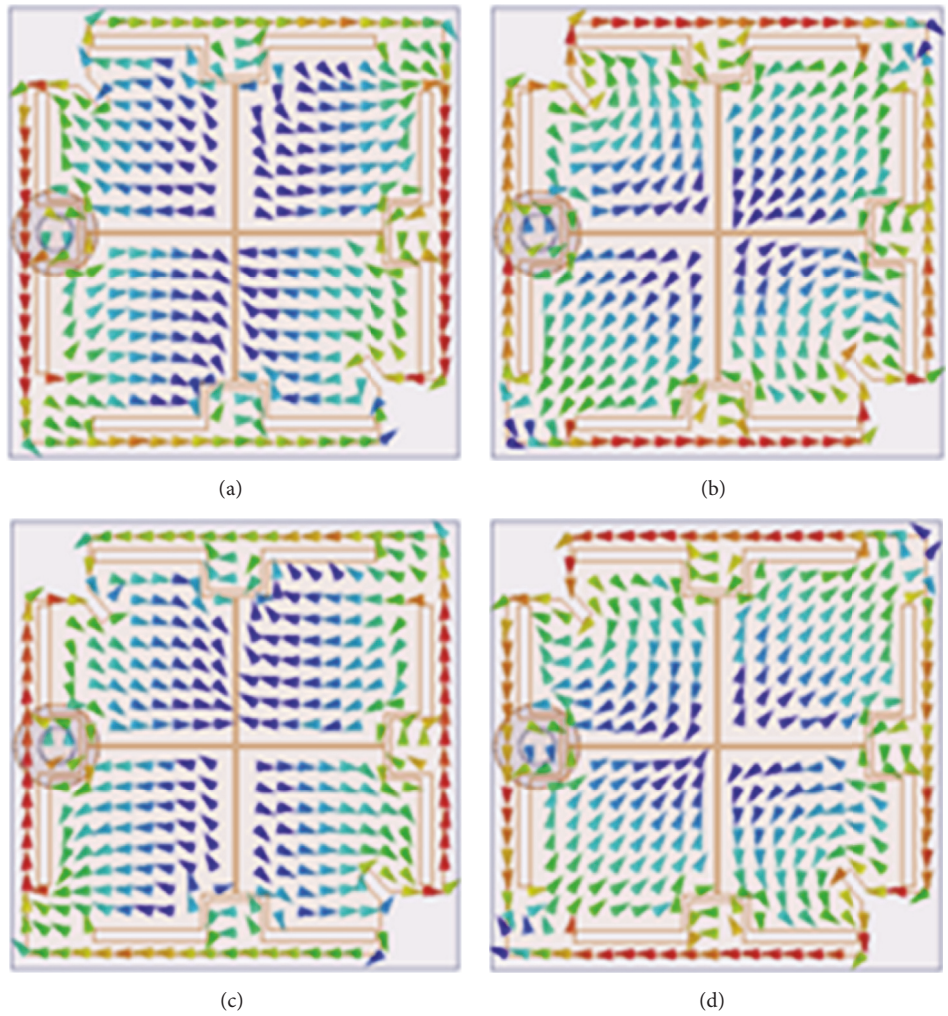

Figure 10: The current distribution of the proposed antenna at 915 MHz: (a) $t = 0$; (b) $t = T/4$; (c) $t = T/2$; (d) $t = 3T/4$.

Table 3: Performance comparison of implantable antennas.

Ref.	Bands (MHz)	Axial ratio bandwidth (MHz)	Volume (mm^3)	Miniaturized methods		
				Dielectric material	Shorting	Radiator structure
[5]	2400–2480	21	1402.4	Taconic	Yes	Capacitive loading
[6]	2400–2480	800	361.9	Rogers 3010	—	Capacitive loading
[7]	402–405	—	399.0	Alumina	Yes	Multilayer
[9]	402–405	—	643.0	Rogers 3210	Yes	π-shaped patch and multilayer
[8]	402–405	—	10240.0	Rogers 3210	Yes	Spiral patch
[11]	902–928	161	248.9	Rogers 3010	Yes	Loop
[12]	902–928	—	486.4	FR4	Yes	J-shaped patch
This work	902–928	14	285.7	Rogers 3010	—	Loading stubs

pin we proposed can achieve miniaturization, which can decrease the influences on neighboring circuits. After optimization, the compact size of $15 \times 15 \times 1.27\ mm^3$ is obtained by utilizing the miniaturized technology of loading stubs and employing meandering slots. Moreover, the proposed antenna can achieve 65% size reduction in contrast with the conventional loop antenna with perturbations. Furthermore, by truncating diagonal corners to turn the perturbation elements, we can generate the orthogonal liner polarized waves. Thus, the right-handed circular polarization (RHCP) is well implemented in different radiation directions. The realized gain of the proposed antenna reaches −27 dBic. It should be noticed that the variation of the implanted depth also has significant impacts on the realized gain. The issue

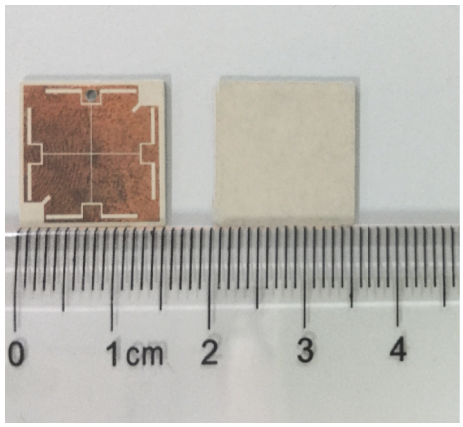

(a)

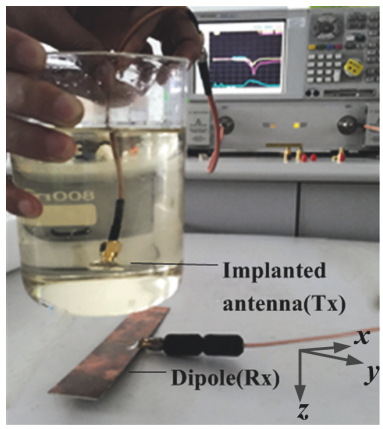

(b)

Figure 11: (a) The prototype of the fabricated antenna; (b) illustration of the measurement setup.

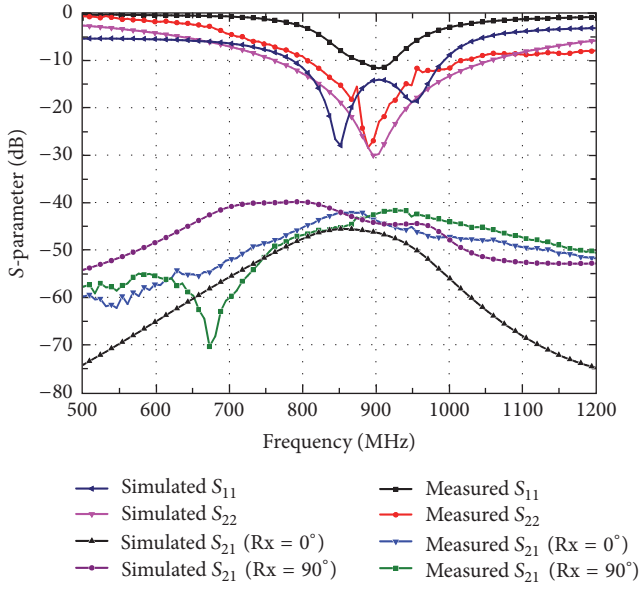

Figure 12: Measured S-parameters of the proposed antenna and the dipole antenna.

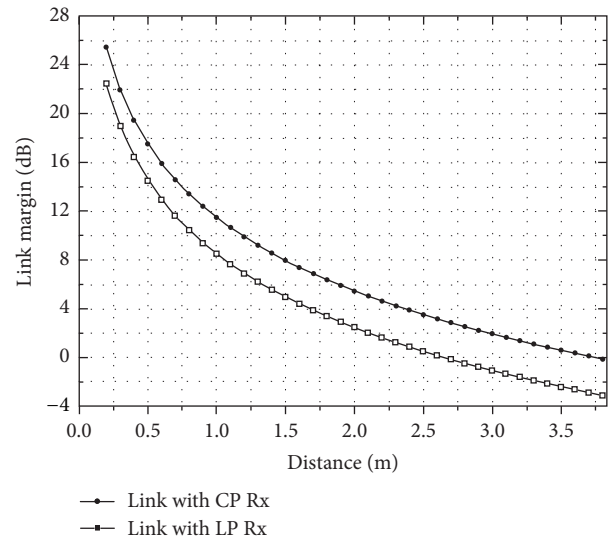

Figure 13: The simulated link margin of the proposed antenna.

of SAR is also discussed and the harm of radiation should not be a concern. Furthermore, the measurement setup of the communication link between the proposed antenna and the external antenna is performed, and the good performance of receiving characteristic is the visual proof of CP property. Finally, the link margin for the proposed antenna is discussed to characterize the wireless communication ability.

Conflicts of Interest

The authors declare that there are no conflicts of interest regarding the publication of this paper.

Acknowledgments

This work was supported in part by the Natural Science Foundation of Jiangsu Province under Grant no. BK20130326, in part by the National Natural Science Foundation of China under Grant nos. 61301076, 61601315, and 61671315, in part by the Open Research Program of State Key Laboratory of Millimeter Waves in China under Grant no. K201417, and in part by Natural Science Fund for colleges and universities in Jiangsu Province under Grant no. 16KJB510039.

References

[1] P. S. Hall and Y. Hao, *Antennas and Propagation for Body-Centric Wireless Communications*, Artech House, Norwell, Mass, USA, 2006.

[2] A. Kiourti and K. S. Nikita, "A review of implantable patch antennas for biomedical telemetry: challenges and solutions," *IEEE Antennas and Propagation Magazine*, vol. 54, no. 3, pp. 210–228, 2012.

[3] H. Li, Y.-X. Guo, and S.-Q. Xiao, "Broadband circularly polarised implantable antenna for biomedical applications," *Electronics Letters*, vol. 52, no. 7, pp. 504–506, 2016.

[4] W. Xia, K. Saito, M. Takahashi, and K. Ito, "Performances of an implanted cavity slot antenna embedded in the human arm," *IEEE Transactions on Antennas and Propagation*, vol. 57, no. 4, pp. 894–899, 2009.

[5] H. Wong, K. K. So, K. B. Ng, K. M. Luk, C. H. Chan, and Q. Xue, "Virtually shorted patch antenna for circular polarization," *IEEE Antennas and Wireless Propagation Letters*, vol. 9, pp. 1213–1216, 2010.

[6] C. Liu, Y.-X. Guo, and S. Xiao, "Circularly polarized helical antenna for ISM-band ingestible capsule endoscope systems," *IEEE Transactions on Antennas and Propagation*, vol. 62, no. 12, pp. 6027–6039, 2014.

[7] F. Merli, L. Bolomey, J.-F. Zürcher, G. Corradini, E. Meurville, and A. K. Skrivervik, "Design, realization and measurements of a miniature antenna for implantable wireless communication systems," *IEEE Transactions on Antennas and Propagation*, vol. 59, no. 10, pp. 3544–3555, 2011.

[8] J. Kim and Y. Rahmat-Samii, "Implanted antennas inside a human body: simulations, designs, and characterizations," *IEEE Transactions on Microwave Theory and Techniques*, vol. 52, no. 8, pp. 1934–1943, 2004.

[9] C.-M. Lee, T.-C. Yo, F.-J. Huang, and C.-H. Luo, "Dual-resonant π-shape with double L-strips PIFA for implantable biotelemetry," *Electronics Letters*, vol. 44, no. 14, pp. 837–839, 2008.

[10] C. Liu, Y.-X. Guo, and S. Xiao, "Capacitively loaded circularly polarized implantable patch antenna for ISM band biomedical applications," *IEEE Transactions on Antennas and Propagation*, vol. 62, no. 5, pp. 2407–2417, 2014.

[11] L.-J. Xu, Y.-X. Guo, and W. Wu, "Miniaturized circularly polarized loop antenna for biomedical applications," *IEEE Transactions on Antennas and Propagation*, vol. 63, no. 3, pp. 922–930, 2015.

[12] M. S. Islam, K. P. Esselle, D. Bull, and P. M. Pilowsky, "Converting a wireless biotelemetry system to an implantable system through antenna redesign," *IEEE Transactions on Microwave Theory and Techniques*, vol. 62, no. 9, pp. 1890–1897, 2014.

[13] A. Karampatzakis, S. Kühn, G. Tsanidis, E. Neufeld, T. Samaras, and N. Kuster, "Antenna design and tissue parameters considerations for an improved modelling of microwave ablation in the liver," *Physics in Medicine and Biology*, vol. 58, no. 10, pp. 3191–3206, 2013.

[14] S. Gao, Q. Luo, and F. Zhu, *Circularly Polarized Antennas*, John Wiley & Sons, 2014.

[15] K.-K. M. Cheng and F.-L. Wong, "A novel approach to the design and implementation of dual-band compact planar 90° branch-line coupler," *IEEE Transactions on Microwave Theory and Techniques*, vol. 52, no. 11, pp. 2458–2463, 2004.

[16] P. Soontornpipit, C. M. Furse, and Y. C. Chung, "Design of implantable microstrip antenna for communication with medical implants," *IEEE Transactions on Microwave Theory and Techniques*, vol. 52, no. 8, pp. 1944–1951, 2004.

[17] T. Karacolak, R. Cooper, J. Butler, S. Fisher, and E. Topsakal, "In vivo verification of implantable antennas using rats as model animals," *IEEE Antennas and Wireless Propagation Letters*, vol. 9, pp. 334–337, 2010.

[18] FCC Std, "OET Bulletin 65, Edition 97-01, Supplement C," 2001.

[19] Z. Duan, Y.-X. Guo, R.-F. Xue, M. Je, and D.-L. Kwong, "Differentially fed dual-band implantable antenna for biomedical applications," *IEEE Transactions on Antennas and Propagation*, vol. 60, no. 12, pp. 5587–5595, 2012.